Atmos. Meas. Tech. Discuss., 7, 9453–9479, 2014
www.atmos-meas-tech-discuss.net/7/9453/2014/
doi:10.5194/amtd-7-9453-2014

Atmospheric Measurement Techniques Discussions

Measurements of $CH_3O_2NO_2$ in the upper troposphere

B. A. Nault[1], C. Garland[2], S. E. Pusede[2,*], P. J. Wooldridge[2], K. Ullmann[3], S. R. Hall[3], and R. C. Cohen[1,2]

[1]Department of Earth and Planetary Science, University of California at Berkeley, Berkeley, CA, USA
[2]Department of Chemistry, University of California at Berkeley, Berkeley, CA, USA
[3]Atmospheric Chemistry Division, National Center for Atmospheric Research, Boulder, CO, USA
[*]now at: NASA Langley Research Center, Hampton, VA, USA

Received: 2 September 2014 – Accepted: 10 September 2014
– Published: 17 September 2014

Correspondence to: R. C. Cohen (rccohen@berkeley.edu)

Published by Copernicus Publications on behalf of the European Geosciences Union.

Abstract

The non-acyl peroxy nitrates, HO_2NO_2 and $CH_3O_2NO_2$, are predicted to be important for photochemistry at low temperatures characteristic of the upper troposphere. We report the first measurements of methyl peroxy nitrate ($CH_3O_2NO_2$). During the Deep Convective Clouds and Chemistry (DC-3) and the Studies of Emissions and Atmospheric Composition, Clouds, and Climate Coupling by Regional Surveys (SEAC4RS) experiments, different inlet configurations for the UC Berkeley Thermal Dissociation-Laser Induced Instrument were tested to optimize measurements of $CH_3O_2NO_2$ from the NASA DC-8. In addition, the inlet modifications were optimized for measurements of NO_2 without $CH_3O_2NO_2$ interferences. The $CH_3O_2NO_2$ measurements we report have a detection limit ($S/N = 2$) of 15 pptv (parts per trillion by volume) at 1 min averaging on a background of 200 pptv NO_2 and an accuracy of ±40 %. Both observations and theoretical calculations were used to constrain the interference of pernitric acid (HO_2NO_2), which partially decomposes (~ 11 %) along with $CH_3O_2NO_2$ in our heated $CH_3O_2NO_2$ channel. Evaluation of the accuracy of the $CH_3O_2NO_2$ measurements is presented.

1 Introduction

Non-acyl peroxy nitrates, such as pernitric acid (HO_2NO_2) and methyl peroxy nitrate ($CH_3O_2NO_2$), have lower thermal stability and shorter lifetimes than acetyl peroxy nitrates such as peroxy acetyl nitrate (PAN) and peroxy proionyl nitrate (PPN). Both classes of peroxy nitrates are temporary reservoirs of NO_x ($NO_x \equiv NO + NO_2$) and in that role indirectly modulate the rate of ozone production.

The non-acyl peroxy nitrates, HO_2NO_2 (thermal lifetime at 300 K of less than 1 min) and $CH_3O_2NO_2$ (thermal lifetime at 300 K of less than 1 s), are most important to the chemistry of the troposphere at low temperatures (below ~ 260 K for HO_2NO_2 and below ~ 240 K for $CH_3O_2NO_2$, to the right of the black line in Fig. 1) (Slusher et al.,

AMTD
7, 9453–9479, 2014

2002; Murphy et al., 2004; Kim et al., 2007; Browne et al., 2011) and at high NO_x mixing ratios (Spencer et al., 2009). HO_2NO_2 is also important for the chemistry of the stratosphere (e.g., Wennberg et al., 1999). The non-acyl peroxy nitrates are produced through the reaction of the methyl peroxy radical or hydroperoxy radical with nitrogen dioxide (Reactions R1 and R2). More complex analogs exist, such as ethyl peroxy nitrate and acetone peroxy nitrate, but their abundance in the atmosphere is expected to be much lower than HO_2NO_2 or $CH_3O_2NO_2$ (e.g., Murphy et al., 2004; Browne et al., 2011). Laboratory experiments have shown these more complex analogs have similar thermal lifetimes to $CH_3O_2NO_2$ (e.g., Zabel et al., 1989; Elfers et al., 1990; Sehested et al., 1998).

Peroxy nitrates are chemically destroyed by thermal decomposition (the reverse of Reactions R1 and R2) followed by reaction of the peroxy radical with NO or HO_2. Photolysis, including near-IR wavelengths for HO_2NO_2, and the reaction of OH with HO_2NO_2 are additional loss mechanisms (Reactions R3–R5).

$$CH_3O_2 + NO_2 + M \leftrightarrow CH_3O_2NO_2 + M \quad \text{(R1)}$$

$$HO_2 + NO_2 + M \leftrightarrow HO_2NO_2 + M \quad \text{(R2)}$$

$$HO_2NO_2(CH_3O_2NO_2) + h\nu \rightarrow HO_2(CH_3O_2) + NO_2 \quad \text{(R3)}$$

$$\text{or} \rightarrow OH(CH_3O) + NO_3 \quad \text{(R4)}$$

$$HO_2NO_2 + OH \rightarrow H_2O + NO_2 + O_2 \quad \text{(R5)}$$

In the upper troposphere (temperature ~ 225 K), HO_2NO_2 has a shorter lifetime (~ 7 h) than $CH_3O_2NO_2$ (~ 15 h) during the daytime due to photolysis and photooxidation (Reactions R3–R5) while at nighttime, $CH_3O_2NO_2$ has a shorter lifetime (~ 22 h) than HO_2NO_2 (~ 540 h) due to thermal stability (Reactions R1–R2).

Browne et al. (2011) investigated the role of $CH_3O_2NO_2$ for NO_x and O_3 chemistry using the GEOS-Chem global chemical transport model. They showed that at temperatures less than 240 K, including the $CH_3O_2NO_2$ chemistry in the model decreases NO_x by an amount ranging from 14–40 %, HNO_3 by 4–14 %, O_3 by 1–4 %, and OH

AMTD
7, 9453–9479, 2014

by 14–28 % while increasing HO_2 by 10–25 %. These changes are accompanied by 12–70 pptv less NO_x, 15–40 pptv less HNO_3, and 1.3–2.6 ppbv less O_3.

Another impact of non-acyl peroxy nitrates is that they are a possible positive interference to in-situ NO_2 measurements in the upper troposphere because the non-acyl peroxy nitrates dissociate in the instruments' inlet prior to detection of ambient NO_2 (Browne et al., 2011). Browne et al. quantified the $CH_3O_2NO_2$ interference to NO_2 measurements using the UC Berkeley Thermal Dissociation-Laser Induced Fluorescence (TD-LIF) in the NASA DC-8 and the interference was as much as ∼ 43 %, increasing as ambient temperatures decreased in the range 255 to 225 K. As the instrument compares well with other measurements of NO_2 and as the physical mechanism of the interference is understood, it should be presumed that most other NO_2 instruments suffer from the same interferences. Thus, it is essential to either correct the NO_2 for the presence of thermally dissociated non-acyl peroxy nitrates or interpret the NO_2 measurements as XNO_2, where XNO_2 is the sum of ambient NO_2 and some or all of the non-acyl peroxy nitrates (Browne et al., 2011).

In order to make unambiguous measurements of NO_2 and $CH_3O_2NO_2$, we developed new configurations of the TD-LIF inlet. In this paper, we describe the design and performance of the modified inlet, provide recommendations for minimizing and eliminating $CH_3O_2NO_2$ interference with NO_2, and present observations of $CH_3O_2NO_2$ from DC-3 and SEAC4RS. These measurements are the first to isolate $CH_3O_2NO_2$ directly.

2 Thermal dissociation-laser induced fluorescence detection of $CH_3O_2NO_2$

2.1 Thermal dissociation-laser induced fluorescence

The TD-LIF instrument has been described previously (Thornton et al., 2000; Day et al., 2002; Wooldridge et al., 2010). Briefly, NO_2 is measured by laser induced fluorescence (Thornton et al., 2000) with supersonic expansion (Cleary et al., 2002). A 7 kHz, Q-switched, frequency doubled Nd:Yag laser pumps a tunable dye laser producing

AMTD
7, 9453–9479, 2014

$\sim$ 20 ns pulses at 585 nm and a bandwidth of 0.06 cm^{-1}. The laser light is focused through two multipass White cells. Red-shifted fluorescence (wavelengths greater than 700 nm) from the excited NO_2 molecules is detected at a right angle to the excitation using a red sensitive photomultiplier tube (Hamamatsu H7421-50). Scattered light is eliminated using time gated detection and dielectric band pass filters that block light at wavelengths less than 700 nm. Fluorescence counts are collected at 4 Hz and recorded as one second averages. The dye laser is tuned on (9 s) and off (3 s) an isolated rovibronic feature of the jet-cooled NO_2 at 585 nm. The ratio between the peak and background NO_2 fluorescence is 10 : 1 sampling from 1 atm ambient pressure. Calibration is performed at least every hour during a level flight leg or after a significant change in altitude using a 4.67 ($\pm$0.26) ppmv NO_2 standard (Praxair) diluted to $\sim$ 2–8 ppbv in zero air. The accuracy and stability of the reference is compared against a library of other NO_2 standards in our laboratory on a regular basis. Fluorescence quenching by water vapor (Thornton et al., 2000) is estimated using the Diode Laser Hygrometer (DLH) measurements of H_2O (Sachse et al., 1987; Diskin et al., 2002).

The TD-LIF instrument used here had two detection cells. A large flow is brought from the undisturbed free stream either by ram pressure from a partially plugged shroud at the inlet tip (ARCTAS, DC-3), or by a 120 L min^{-1} sample pump (SEAC4RS). The core of that flow was subsampled by a short ($\sim$ 0.10 m long) tube where air had a residence time of $\sim$ 0.03 s and then split into multiple sample lines for detection of specific categories of NO_y (Fig. 2). For $CH_3O_2NO_2$ detection, the sample is passed directly through a heated quartz tube (internal diameter $\sim$ 4.3 mm, $T \approx 60\,^{\circ}C$) for 0.06–0.08 s followed by PFA tubing (i.d. $\sim$ 3.2 mm) to the NO_2 detection cell. The residence time between the heater and the detector is $\sim$ 0.4–0.5 s. The temperature ($\sim 60\,^{\circ}C$) for the heated quartz was determined by calculating the temperature that would maximize the amount of $CH_3O_2NO_2$ dissociated while minimizing the amount of HO_2NO_2 dissociated (Fig. 3). This also ensures that PAN and its analogs (e.g., PPN) did not dissociate in the $CH_3O_2NO_2$ channel. N_2O_5 has similar thermodynamics to HO_2NO_2 at this temperature (Wooldridge et al., 2010); however, typically the N_2O_5 mixing ratio during the

AMTD
7, 9453–9479, 2014

day is negligible due to the short lifetime of the NO_3 radical, making it an unimportant interference. Also, we chose the temperature set point based on a scan of air containing acyl peroxy nitrates and non-acyl peroxy nitrates. The mixing ratio of ambient $CH_3O_2NO_2$ is determined by subtracting the measurements from the NO_2 channel from the $CH_3O_2NO_2$ channel (60 °C, Fig. 4). Similarly, the mixing ratio of ambient sum of peroxy nitrates ($\Sigma PNs = PAN + PPN + CH_3O_2NO_2 + HO_2NO_2 + \ldots$) is determined by subtracting the measurements from the NO_2 channel from the ΣPNs channel, and the mixing ratio of ambient sum of alkyl and multifunctional nitrates (ΣANs) is determined by subtracting the measurements from the ΣPNs channel from the ΣANs channel (Fig. 4).

2.2 Interference free NO_2 measurements

Measuring NO_2 free of $CH_3O_2NO_2$ interference is desirable for understanding upper tropospheric chemistry and essential to correctly derive the $CH_3O_2NO_2$ and ΣPNs mixing ratios from the heated channels (Fig. 4). Measurements of NO_2 at ambient temperatures lower than 240 K, where non-acyl peroxy nitrates are more abundant due to longer thermal lifetimes (Fig. 1), are not free of interferences if the sample residence time in the aircraft is long (Browne et al., 2011). Figure 5 shows the fraction of $CH_3O_2NO_2$ and HO_2NO_2 thermally dissociating in the NO_2 inlet prior to measuring NO_2 for different residence times and as a function of cabin temperature. At a cabin temperature of 300 K, approximately 90^{+5}_{-10} %, 40^{+11}_{-6} % and 10^{+3}_{-2} % of $CH_3O_2NO_2$ and approximately 8 ± 2 %, 2 %, and less than 1 % of HO_2NO_2 will thermally decompose at residence times of 2 s, 0.5 s, and 0.1 s, respectively. The uncertainties are based on the 2σ range reported for the decomposition rates of $CH_3O_2NO_2$ and HO_2NO_2. Eliminating the influence of $CH_3O_2NO_2$ and HO_2NO_2 on the observations thus NO_2 requires residence times of less than 0.1 s.

AMTD
7, 9453–9479, 2014

2.3 Inlet configurations and effects on NO_2 and $CH_3O_2NO_2$ measurements

Figure 2 shows the schematic of the TD-LIF inlet. Table 1 has the lengths and residence times of the different inlets used in three recent experiments: ARCTAS, DC-3, and SEAC4RS. The residence time is set by the measured length of tubing, the diameter of the tubing, and the flow speed of the sample pumps. Unless stated otherwise, the tubing has an internal diameter of approximately 3.2 mm. Following the recommendations of Wooldridge et al. (2010) and Browne et al. (2011), we shortened the residence time for the NO_2 sample after the ARCTAS experiment for the DC-3 experiment to make interference free NO_2 measurements. In ARCTAS, the NO_2 channel went through 0.2 m of tubing heated to $\sim 50\,^{\circ}C$ (Section B) and then through 2 m unheated tubing (Section C) to the LIF cell (Fig. 2). For DC-3, we reduced Section B from 0.2 to 0.08 m, reducing the amount of time the NO_2 sample is heated to $50\,^{\circ}C$. Also, we reduced Section C from 2 to 1.5 m. This reduced the maximum residence time for NO_2 from 0.85 to 0.5 s. For typical cabin temperatures of 300 K, approximately 42 % of $CH_3O_2NO_2$ still decomposes in the NO_2 channel at 0.5 s residence time.

After examining the results from the DC-3 configuration, we reduced the length and residence time to further minimize the thermal decomposition of $CH_3O_2NO_2$ in the unheated NO_2 channel. For SEAC4RS, we used a bypass pump to bring large flow of ambient air as near to the NO_2 detection cell as possible, thereby reducing the NO_2 sample residence time. We also moved the dissociation heaters from near the window inlet to near the LIF cells, increasing the length of Section A from 0.1 to 1 m and reducing Section C from 1.5 to 0.3 m. Also, the Section A internal diameter went from $\sim$ 3.2 to 15.9 mm. Finally, Section B slightly increased from 0.08 to 0.12 m; however, Section B was not heated for SEAC4RS. The combined reduction of the overall tubing length was small, from 1.68 to 1.42 m, but the added sample pump reduced the maximum residence time from 0.5 s (DC-3) to 0.23 s (SEAC4RS). This reduced the fractional thermal dissociation of $CH_3O_2NO_2$ in the NO_2 channel from approximately 42 % to approximately 22 %.

AMTD
7, 9453–9479, 2014

We obtain an NO_2 measurement by correcting for the partial thermal dissociation of $CH_3O_2NO_2$ in the XNO_2 channel (Eq. 1) and $CH_3O_2NO_2$ by subtracting NO_2 and the fractional thermally dissociated HO_2NO_2 from the $CH_3O_2NO_{2,CHANNEL}$ (Eq. 2).

$$XNO_2 = NO_2 + f_1 \cdot CH_3O_2NO_2 \quad (1)$$

$$CH_3O_2NO_{2,CHANNEL} = NO_2 + CH_3O_2NO_2 + f_2 \cdot HO_2NO_2 \quad (2)$$

We use the cabin temperature we measured near the TD-LIF NO_2 sample line along with the thermal rate constant (Table 2) to calculate the fraction of $CH_3O_2NO_2$ (f_1 in Eq. 1) that dissociates in the NO_2 sample line. We use the measured oven temperature ($\sim 60\,^{\circ}C$) along with the thermal rate constant (Table 2) to calculate the fraction of HO_2NO_2 (f_2 in Eq. 2) that has dissociated in the $CH_3O_2NO_2$ channel. With the two Eqs. (1) and (2), we can solve for the NO_2 and $CH_3O_2NO_2$ mixing ratios observed if there is an independent measurement or calculation of HO_2NO_2. During DC-3, the correction for the thermal dissociation of $CH_3O_2NO_2$ in XNO_2 ranged from a 0 to 17 pptv (0–40 %) of the NO_2 mixing ratios at temperatures less than 240 K. During SEAC4RS, the correction ranged from 0 to 23 pptv (0–21 %).

2.4 Accuracy, uncertainty and limit of detection for $CH_3O_2NO_2$

The accuracy of the $CH_3O_2NO_2$ measurements depends on the accuracy of our primary measurement of NO_2, the conversion efficiency in our inlet, and the interference of HO_2NO_2 dissociating with $CH_3O_2NO_2$. The uncertainty of the NO_2 calibration standard is ~ 5 % (Sect. 2.1). Using the rate constant and 2σ uncertainty recommendation from JPL-2011 (Sander et al., 2011) at 60 °C, the thermal decomposition rate constant of $CH_3O_2NO_2$ is $36.0^{+19.0}_{-13.0}\,s^{-1}$, indicating between 85–99 % of $CH_3O_2NO_2$ is decomposed at this temperature and a residence time of 0.08 s. Including the uncertainty estimated for the oven temperature (±5 °C), the amount of $CH_3O_2NO_2$ decomposed is 70–100 %.

The similarity in the bond strength between HO_2NO_2 and $CH_3O_2NO_2$ (~ 100 and $\sim 93\,kJ\,mol^{-1}$, respectively) prevents having a temperature set point that completely

AMTD
7, 9453–9479, 2014

separates the two species (Fig. 3). For the oven temperature selected to decompose $CH_3O_2NO_2$ (60 °C) and the residence time in the oven (0.08 s), we calculate approximately 11^{+10}_{-6} % of HO_2NO_2 dissociates in the $CH_3O_2NO_2$ channel. Combining the uncertainties from thermal decomposition of $CH_3O_2NO_2$ and the fractional thermal decomposition of HO_2NO_2 in the $CH_3O_2NO_2$ oven, we estimate the accuracy of the $CH_3O_2NO_2$ measurements to be ±40 %. We note that the sum of the NO_2 and $CH_3O_2NO_2$ measurement ($CH_3O_2NO_{2,CHANNEL}$) is more accurate (~ 5 %) than the separate quantities.

The precision of the $CH_3O_2NO_2$ measurements depends on the shot noise of the photon counting rate, the precision of the NO_2 measurement, the concentration of NO_2, and the concentration of $CH_3O_2NO_2$. Using the median NO_2 measured between 10 and 11 km (~ 200 pptv of NO_2), and using the lower end of the sensitivity observed during DC-3 (0.100 cts pptv^{-1}), the detection limit for $CH_3O_2NO_2$ is 15 pptv at 60 s^{-1} for $S/N = 2$. The median limit of detection ($S/N = 2$ and 60 s averaged data) for the DC-3 campaign is shown vs. altitude in Fig. 7b (red line).

3 Ambient measurements of $CH_3O_2NO_2$

$CH_3O_2NO_2$ measurements were obtained during the DC-3 (2012) and SEAC4RS (2013) campaigns. All data used is located in the NASA public archives for these two missions (http://www-air.larc.nasa.gov/cgi-bin/ArcView/dc3-seac4rs and https://www-air.larc.nasa.gov/cgi-bin/ArcView/seac4rs).

A time series of $CH_3O_2NO_2$ during the flight of 30 May 2012 is shown in Fig. 6. HO_2NO_2 measured (grey line) by chemical ionization-mass spectrometry (Kim et al., 2007) and calculated at instantaneous photostationary steady state (Eq. 3, red line) are also shown in the figure. The reactions included in the photostationary steady state calculations for HO_2NO_2 are shown in Table 2, and the calculations were constrained to the measured values in Table 3. We constrain our observations to solar zenith angles

AMTD
7, 9453–9479, 2014

less than 85° and HO_2NO_2 lifetime less than 12 h.

$$[HO_2NO_2] = \frac{k_2[HO_2][NO_2]}{j_1 + j_2 + k_{-2} + k_3[OH]} \quad (3)$$

Kim et al. (2007) observed that instantaneous photostationary steady state calculations were approximately a factor of 2 higher than observations. In Kim et al. (2007), the authors concluded the factor of ~ 2 is due to HO_2NO_2 and HO_x measurements not being consistent with our current understanding of photochemistry in the upper troposphere stemming from either unknown uncertainties in the measurements, the formation is too fast, or the loss is too slow. We observe a similar result; therefore, we divide the calculations by 2 to reflect that result.

As seen in Fig. 6, between the time 7.5 and 8×10^4 s, $CH_3O_2NO_2$ is fluctuating near the limit of detection (0–50 pptv), whereas HO_2NO_2 spikes in both the measurement and steady state calculations. During this time, the $CH_3O_2NO_2$ lifetime is less than 10 min, indicating the $CH_3O_2NO_2$ mixing ratios should be low. We utilize these observations to calculate an upper limit for the thermal dissociation of HO_2NO_2 in the $CH_3O_2NO_2$ channel. The median measured and calculated HO_2NO_2 are 94^{+11}_{-35} and 78^{+20}_{-4} pptv (plus 75th quartile and minus 25th quartile), respectively. In the $CH_3O_2NO_2$ channel, we observed 24^{+10}_{-6} pptv (median and inter-quartile). Assuming zero for the $CH_3O_2NO_2$ mixing ratio, this gives an upper limit to the HO_2NO_2 present in the $CH_3O_2NO_2$ channel of ~ 25 % (observed) and ~ 30 % (calculated) HO_2NO_2 thermally dissociated. Calculations (Sect. 2.4) suggest the most likely amount of HO_2NO_2 thermally dissociated is ~ 11 % with an upper limit based on propagating uncertainties in rate constants of 25 to 30 %. The observed values are consistent with this upper limit. We conclude that some (~ 6 pptv calculated assuming photostationary steady state similar to Browne et al., 2011) $CH_3O_2NO_2$ should be present. If we assume this $CH_3O_2NO_2$ is correct, the HO_2NO_2 fraction dissociated is 19–23 %.

Figure 6 also shows the altitude (blue) and temperature (green) during the 30 May 2012 flight. The dips in the $CH_3O_2NO_2$ measurements that occur around 8×10^4 s

AMTD
7, 9453–9479, 2014

and 8.5–9 × 10^4 s correspond to measurements taken at lower altitudes and thus higher temperatures. These measurements were taken in air where $CH_3O_2NO_2$ lifetimes were less than 1 h. Higher $CH_3O_2NO_2$ mixing ratios occur at higher altitudes (colder temperatures), corresponding to $CH_3O_2NO_2$ lifetimes greater than 10 h.

$CH_3O_2NO_2$'s dependence on temperature and altitude is also seen in Fig. 7b which shows the median $CH_3O_2NO_2$ profile during DC-3 (black) and SEAC4RS (dark grey) along with the median $CH_3O_2NO_2$ profile from ARCTAS-A (blue, as calculated by Browne et al., 2011). At altitudes above 7 km, higher mixing ratios of $CH_3O_2NO_2$ were observed during both DC-3 and SEAC4RS compared to ARCTAS-A due to the influence of deep convection, lightning NO_x, and biomass burning. Also, DC-3 and SEAC4RS occurred later in the year (May–June 2012 for DC-3 and August–September 2013 for SEAC4RS) than ARCTAS-A (April 2008); thus, photochemistry is more active, producing more $CH_3O_2NO_2$. This is consistent with Browne et al. (2011), who calculated that $CH_3O_2NO_2$ mixing ratios are higher in the summer than spring. Finally, $CH_3O_2NO_2$ during SEAC4RS at lower altitudes is higher due to the impact of agricultural and biomass burning. Higher NO_2 mixing ratios from biomass burning shift the equilibrium towards $CH_3O_2NO_2$, similar to the higher NO_2 concentrations shifting the equilibrium towards HO_2NO_2 production near an urban area (Spencer et al., 2009). Higher $CH_3O_2NO_2$ mixing ratios due to biomass burning are also consistent to the GEOS-Chem results from Browne et al. (2011). Even though temperatures in the lower stratosphere are low enough for the $CH_3O_2NO_2$ lifetime to be greater than 10 h, the lower stratosphere has lower mixing ratios of the precursors (e.g., acetaldehyde) that produce methyl peroxy radicals, resulting in low mixing ratios of $CH_3O_2NO_2$ (Fig. 6 after 9 × 10^4 s and Fig. 7b above 11.5 km during DC-3).

To evaluate the $CH_3O_2NO_2$ measurement, we compare inferred $CH_3O_2NO_2$ ($\Delta CH_3O_2NO_2 \equiv \Sigma PNs - (HO_2NO_2 + PAN + PPN)$) to measured $CH_3O_2NO_2$ during the DC-3 campaign (Fig. 8). PAN, PPN, and HO_2NO_2 were measured by chemical ionization-mass spectrometry (Slusher et al., 2004; Kim et al., 2007). The observations are one minute merged data from temperatures between 220 and 230 K.

AMTD
7, 9453–9479, 2014

Using a weighted bivariate least-squares (Cantrell, 2008), we calculated a slope of 0.93 (±0.07) after removing the $\Delta CH_3O_2NO_2$ population greater than 400 pptv ($\Delta CH_3O_2NO_2$ observations that are ±3 standard deviation of the median value). Using photostationary state HO_2NO_2, we calculate a slope of 1.11 (±0.08) (not shown). While not completely independent approaches, the two methods of $CH_3O_2NO_2$ are sufficiently independent to suggest the direct $CH_3O_2NO_2$ measurement is accurate to at least the ±40 % estimate above.

4 Discussion

In prior analysis of tropospheric air cooler than 240 K, Murphy et al. (2004) calculated the sum of HO_2NO_2 and $CH_3O_2NO_2$ as the difference between ΣPNs measured by TD-LIF and PAN and PPN measured using gas chromatography with electron capture detection (similar to $\Delta CH_3O_2NO_2$ above). Murphy et al. reported these two species were a large fraction of the NO_y budget at temperatures cooler than 240 K (17–22 %), impacting NO_x and radical chemistry. Between 220 and 230 K during DC-3, $CH_3O_2NO_2$ composed 7 % and HO_2NO_2 composed 5 ± 2 % of the median NO_y budget, where NO_y is defined as the sum of NO_x, ΣPNs, ΣANs, and HNO_3. This is significant since many transport models neglect $CH_3O_2NO_2$ chemistry. During DC-3, these species comprise a larger portion of the median NO_y budget than HNO_3 (4 %), which is a terminal sink for NO_x. The percent composition for the non-acyl peroxy nitrates during DC-3 were lower than Murphy et al.'s (2004) observations because the sampling during DC-3 was biased toward fresh convective outflow impacted by lightning NO_x, meaning NO_x composed 39 % of the NO_y budget vs. the 5 % for the air observed by Murphy et al. (2004). For background air ($NO_x/NO_y < 0.2$) observed during DC-3, $CH_3O_2NO_2$ still composed a larger portion of the median NO_y budget (12 %) than HNO_3 (6 %) and HO_2NO_2 (5 %). The contribution of the non-acyl peroxy nitrates to the background NO_y budget during DC-3 is 17 %, similar to the observations by Murphy et al. (2004) of 17 %.

AMTD
7, 9453–9479, 2014

The lower NO_x mixing ratios characteristic of the air observed by Murphy et al. (2004) were also characteristic of the air observed by Browne et al. (2011) during ARCTAS-A, as both were springtime measurements in the Arctic. The comparison of ARCTAS-A, DC-3, and SEAC4RS is shown in Fig. 7. The lower NO_2 mixing ratios observed during ARCTAS-A meant the air masses were more dominated by $CH_3O_2NO_2$ than by NO_2 ($CH_3O_2NO_2/(NO_2 + CH_3O_2NO_2)$ ratios closer to 1.0, Fig. 7c). In DC-3, the influence of lightning NO_x emissions made the median air masses for the entire campaign more dominated by NO_2 (ratios less than 0.5). The median $CH_3O_2NO_2/(NO_2 + CH_3O_2NO_2)$ ratios are slightly smaller than the ratios calculated in the GEOS-Chem model from Browne et al. (2011) for air influenced by deep convection and lightning. In background air sampled by the NASA DC-8 during DC-3, the median $CH_3O_2NO_2/(NO_2 + CH_3O_2NO_2)$ ratio was in the range 0.3–0.7 (Fig. 7c, green). We observed similar median ratios during SEAC4RS (Fig. 7c, dark grey). These values are closer to the values calculated during ARCTAS (Fig. 7c, blue; Browne et al., 2011). This indicates that as the air ages, the ratio shifts towards air more dominated by $CH_3O_2NO_2$, impacting the ozone chemistry of the upper troposphere, as previously demonstrated by Browne et al. (2011).

5 Conclusions

We report the first measurements of atmospheric $CH_3O_2NO_2$, and we also report recommendations for instrument design to sample NO_2 free of interferences from thermal decomposition of non-acyl peroxy nitrates. We conclude that for an instrument temperature of 300 K, NO_2 sampling times of less than 0.1 s are required to have less than 10 % thermal decomposition of $CH_3O_2NO_2$ and less than 1 % thermal decomposition of HO_2NO_2 in the NO_2 detector. The interference of $CH_3O_2NO_2$ from thermally decomposing in NO_2 sample lines can be corrected with measurements of $CH_3O_2NO_2$. During DC-3 at temperatures less than 230 K, the median $CH_3O_2NO_2$ composed a larger fraction of NO_y than HNO_3. Since HNO_3 is a terminal sink of NO_x while $CH_3O_2NO_2$

AMTD
7, 9453–9479, 2014

is a temporary reservoir of NO_x, $CH_3O_2NO_2$ being more abundant in the upper troposphere further supports the importance of including $CH_3O_2NO_2$ in chemical models. Finally, similar to the GEOS-Chem calculations from Browne et al. (2011), we see increased $CH_3O_2NO_2$ mixing ratios from spring to summer season and increasing $CH_3O_2NO_2$ mixing ratios as temperatures decrease and altitudes increase.

Acknowledgements. This research was funded by NASA grant NNX08AR13G and based upon work supported by the National Science Foundation Graduate Research Fellowship under Grant No. DGE 1106400 to BAN. SEP acknowledges support from the NASA Postdoctoral Program. We thank William H. Brune for use of the OH and HO_2 measurements, L. Gregory Huey for the use of Georgia Institute of Technology CIMS data, Paul O. Wennberg for the use of HNO_3 data, and Thomas B. Ryerson for the use of NO data. We also thank the ground and flight crews of the DC-8 for their hard work and support during DC-3 and SEAC4RS and the DC-3 and SEAC4RS science team for their hard work.

References

Browne, E. C., Perring, A. E., Wooldridge, P. J., Apel, E., Hall, S. R., Huey, L. G., Mao, J., Spencer, K. M., Clair, J. M. St., Weinheimer, A. J., Wisthaler, A., and Cohen, R. C.: Global and regional effects of the photochemistry of $CH_3O_2NO_2$: evidence from ARCTAS, Atmos. Chem. Phys., 11, 4209–4219, doi:10.5194/acp-11-4209-2011, 2011.

Cantrell, C. A.: Technical Note: Review of methods for linear least-squares fitting of data and application to atmospheric chemistry problems, Atmos. Chem. Phys., 8, 5477–5487, doi:10.5194/acp-8-5477-2008, 2008.

Cleary, P. A., Wooldridge, P. J., and Cohen, R. C.: Laser-induced fluorescence detection of atmospheric NO_2 with a commercial diode laser and a supersonic expansion, Appl. Optics, 41, 6950–6956, 2002.

Day, D. A., Wooldridge, P. J., Dillon, M. B., Thornton, J. A., and Cohen, R. C.: A thermal dissociation laser-induced fluorescence instrument for in situ detection of NO_2, peroxy nitrates, alkyl nitrates, and HNO_3, J. Geophys. Res., 107, 4046, doi:10.1029/2001JD000779, 2002.

AMTD
7, 9453–9479, 2014

Diskin, G. S., Podolske, J. R., Sachse, G. W., and Slate, T. A.: Open-path airborne tunable diode laser hygrometer, in: Diode Lasers and Applications in Atmospheric Sensing, edited by: Fried, A., SPIE Proceedings, 4817, 196–204, 2002.

Elfers, G., Zabell, F., and Becker, K. H.: Determination of the rate constant ratio for the reactions of the ethylperoxy radical with NO and NO_2, Chem. Phys. Lett., 168, 14–19, 1990.

Faloona, I. C., Tan, D., Lesher, R. L., Hazen, N. L., Frame, C. L., Simpas, J. B., Harder, H., Martinez, M., Di Carlo, P., Ren, X., and Brune, W. H.: A laser-induced fluorescence instrument for detecting tropospheric OH and HO_2: characteristics and calibration, J. Atmos. Chem., 47, 139–167, 2004.

Jiménez, E., Gierczak, T., Stark, H., Burkholder, J. B., and Ravishankara, A. R.: Reaction of OH with HO_2NO_2 (peroxynitric acid): rate coefficients between 218 and 335 K and product yields at 298 K, J. Phys. Chem. A., 108, 1139–1149, doi:10.1021/jp0363489, 2004.

Kim, S., Huey, L. G., Stickel, R. E., Tanner, D. J., Crawford, J. H., Olson, J. R., Chen, G., Brune, W. H., Ren, X., Lesher, R., Wooldridge, P. J., Bertram, T. H., Perring, A., Cohen, R. C., Lefer, B. L., Shetter, R. E., Avery, M., Diskin, G., and Sokolik, I.: Measurement of HO_2NO_2 in the free troposphere during the Intercontinental Chemical Transport Experiment–North America 2004, J. Geophys. Res., 112, D12S01, doi:10.1029/2006Jd007676, 2007.

Murphy, J. G., Thornton, J. A., Wooldridge, P. J., Day, D. A., Rosen, R. S., Cantrell, C., Shetter, R. E., Lefer, B., and Cohen, R. C.: Measurements of the sum of HO_2NO_2 and $CH_3O_2NO_2$ in the remote troposphere, Atmos. Chem. Phys., 4, 377–384, doi:10.5194/acp-4-377-2004, 2004.

Sachse, G. W., Hill, G. F., Wade, L. O., and Perry, M. G.: Fast response, high precision carbon monoxide sensor using a tunable diode laser absorption technique, J. Geophys. Res., 92, 2071–2081, 1987.

Sander, S. P., Abbatt, J. Barker, J. R., Burkholder, J. B., Friedl, R. R., Golden, D. M., Huie, R. E., Kolb, C. E., Kurylo, M. J., Moortgat, G. K., Orkin, V. L., and Wine, P. H.: Chemical Kinetics and Photochemical Data for Use in Atmospheric Studies, Evaluation Number 17, JPL Publication 10-6, Jet Propulsion Laboratory, Pasadena, 2011.

Sehested, J., Christensen, L. K., Nielsen, O. J., Bilde, M. Wallington, T. J., Schneider, W. F., Orlando, J. J., and Tyndall, G. S.: Atmospheric chemistry of acetone: kinetic study of the $CH_3C(O)CH_2O_2 + NO/NO_2$ reactions and decomposition of $CH_3C(O)CH_2O_2NO_2$, Int. J. Chem. Kinet., 30, 475–489, doi:10.1002/(SICI)1097-4601(1998)30:7<475::AID-KIN4>3.0.CO;2-P, 1998.

AMTD
7, 9453–9479, 2014

Shetter, R. E. and Müller, M.: Photolysis frequency measurements using actinic flux spectroradiometry during the PEM-Tropics Mission: instrument description and some results, J. Geophys. Res., 104, 5647–5661, 1999.
Slusher, D. L., Huey, L. G., Tanner, D. J., Chen, G., Davis, D. D., Buhr, M., Nowak, J. B., Eisele, F. L., Kosciuch, E., Mauldin, R. L., Lefer, B. L., Shetter, R. E., and Dibb, J. E.: Measurements of pernitric acid at the South Pole during ISCAT 2000, Geophys. Res. Lett., 29, 2001, doi:10.1029/2002GL015703, 2002.
Slusher, D., Huey, L. G., Tanner, D. J., Flocke, F. M., and Roberts, J. M.: A thermal dissociation chemical ionization mass spectrometry (TD-CIMS) technique for the simultaneous measurements of peroxacyl nitrates and dinitrogen pentoxide, J. Geophys. Res., 109, D19315, doi:10.1029/2004JD004670, 2004.
Spencer, K. M., McCabe, D. C., Crounse, J. D., Olson, J. R., Crawford, J. H., Weinheimer, A. J., Knapp, D. J., Montzka, D. D., Cantrell, C. A., Hornbrook, R. S., Mauldin III, R. L., and Wennberg, P. O.: Inferring ozone production in an urban atmosphere using measurements of peroxynitric acid, Atmos. Chem. Phys., 9, 3697–3707, doi:10.5194/acp-9-3697-2009, 2009.
Thornton, J. A., Wooldridge, P. J., and Cohen, R. C.: Atmospheric NO_2: in situ laser-induced fluorescence detection at parts per trillion mixing ratios, Anal. Chem., 72, 528–539, 2000.
Wennberg, P. O., Salawitch, R. J., Donaldson, D. J., Hanisco, T. F., Lanzendorf, E. J., Perkins, K. K., Lloyd, S. A., Vaida, V., Gao, R. S., Hintsa, E. J., Cohen, R. C., Swartz, W. H., Kusterer, T. L., and Anderson, D. E.: Twilight observations suggest unknown sources of HO_x, Geophys. Res. Lett., 26, 1373–1376, 1999.
Wooldridge, P. J., Perring, A. E., Bertram, T. H., Flocke, F. M., Roberts, J. M., Singh, H. B., Huey, L. G., Thornton, J. A., Wolfe, G. M., Murphy, J. G., Fry, J. L., Rollins, A. W., LaFranchi, B. W., and Cohen, R. C.: Total Peroxy Nitrates (ΣPNs) in the atmosphere: the Thermal Dissociation-Laser Induced Fluorescence (TD-LIF) technique and comparisons to speciated PAN measurements, Atmos. Meas. Tech., 3, 593–607, doi:10.5194/amt-3-593-2010, 2010.
Zabel, F., Reimer, A., Becker, K. H., and Fink, E. H.: Thermal decomposition of alkyl peroxynitrates, J. Phys. Chem., 93, 5500–5507, 1989.

AMTD
7, 9453–9479, 2014

Table 1. Lengths for tubing in the corresponding sections for Fig. 2.

Campaign	Section A	Section B	Section C	NO_2 Channel Max Residence Time
ARCTAS	0.10 m	0.20 m	2.00 m	0.85 s
DC-3	0.10 m	0.08 m	1.50 m	0.50 s
SEAC4RS	1.00 m	0.12 m	0.30 m	0.23 s

AMTD
7, 9453–9479, 2014

Table 2. Reactions and rates used in calculating dissociations in instrument and photostationary steady state calculations for HO_2NO_2.

Reaction	Rate Constant
$CH_3O_2NO_2 + M \leftrightarrow CH_3O_2 + NO_2 + M$	Low Pressure Limit = $1.0 \times 10^{-30} \times (T/300)^{-4.8}$ High Pressure Limit = $7.2 \times 10^{-12} \times (T/300)^{-2.1}$ $K_{eq} = 9.5 \times 10^{-29} \times \exp(11234/T)$ [a]
$HO_2NO_2 + M \leftrightarrow HO_2 + NO_2 + M$	Low Pressure Limit = $2.0 \times 10^{-31} \times (T/300)^{-3.4}$ High Pressure Limit = $2.9 \times 10^{-12} \times (T/300)^{-1.1}$ $K_{eq} = 2.1 \times 10^{-27} \times \exp(10900/T)$ [a]
$HO_2NO_2 + OH \rightarrow NO_2 + H_2O + O_2$	$8.8 \times 10^{-19} \times T^2 \times \exp(1130/T)$ [b]
$HO_2NO_2 + h\nu \rightarrow HO_2 + NO_2$	Measured $+1 \times 10^{-5}$ [c]
$HO_2NO_2 + h\nu \rightarrow OH + NO_3$	Measured

[a] JPL 2011 (Sander et al., 2011).
[b] Jiménez et al. (2004).
[c] Measured photolysis rate plus IR overtone (Murphy et al., 2004).

AMTD
7, 9453–9479, 2014

Table 3. Measurements used in this analysis and for photostationary steady state calculations for HO_2NO_2.

Species	Method	Reference
NO_2, $CH_3O_2NO_2$, ΣPNs	Thermal dissociation-laser induced fluorescence	Thornton et al. (2000) Day et al. (2002)
HO_2NO_2, PAN, PPN	Chemical ionization mass spectrometry	Slusher et al. (2004) Kim et al. (2007)
OH, HO_2	Laser induced fluorescence	Faloona et al. (2004)
UV photolytic frequencies	Spectral radiometry	Shetter and Müller (1999)

AMTD
7, 9453–9479, 2014

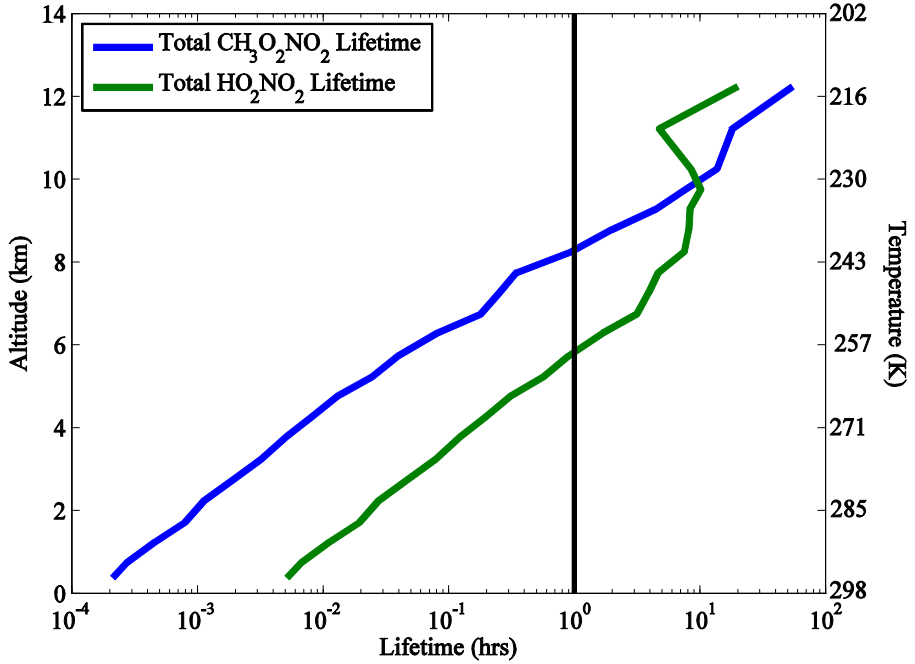

Figure 1. Mean total lifetime profile of $CH_3O_2NO_2$ (blue) and HO_2NO_2 (green) during DC-3 during daytime. The black line is to highlight where the non-acyl peroxy nitrates lifetime is greater than 1 h.

AMTD
7, 9453–9479, 2014

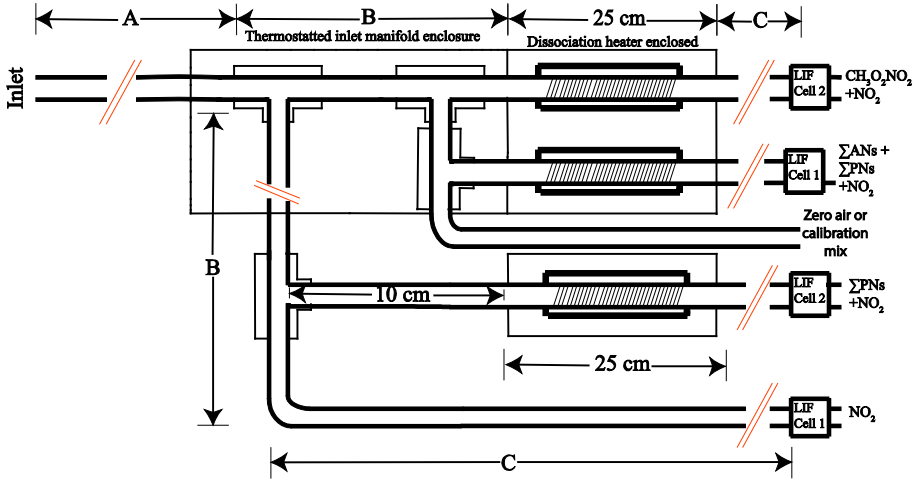

Figure 2. Schematic of the TD-LIF inlet. Arrows and letters refer to lengths referenced in Table 1. The total species measured is shown to the right of the LIF Cells, where $\Sigma PNs \equiv PAN + PPN + CH_3O_2NO_2 + HO_2NO_2 + \ldots$ and $\Sigma ANs \equiv$ alkyl and multifunctional nitrates.

AMTD
7, 9453–9479, 2014

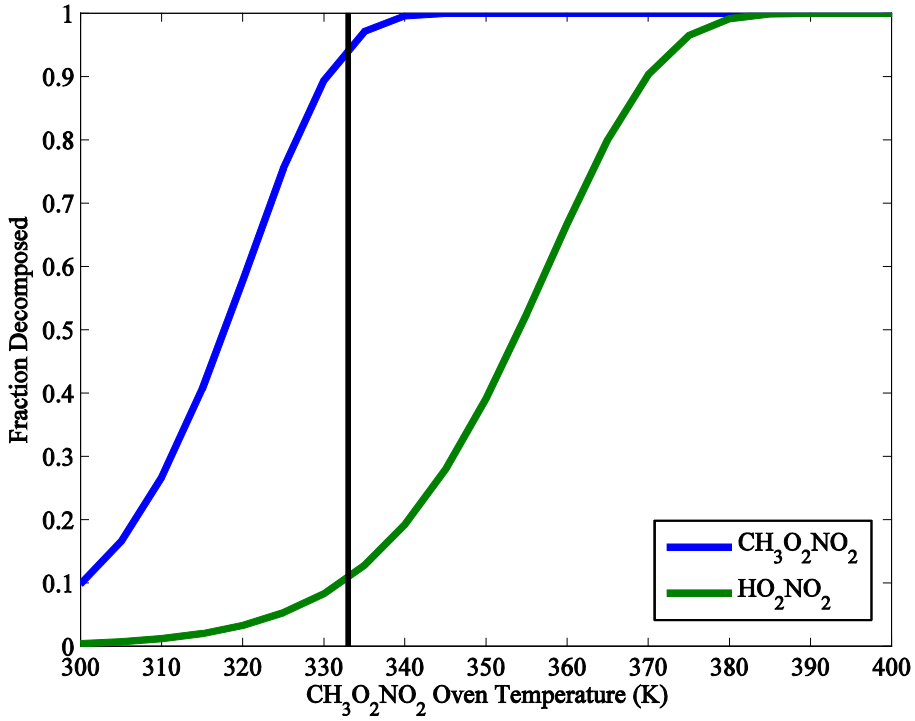

Figure 3. The calculated percent decomposition of non-acyl peroxy nitrates at various $CH_3O_2NO_2$ oven temperatures at a pressure of 230 hPa and a residence time of 0.08 s. The blue line is the percent decomposition of $CH_3O_2NO_2$, and the green line is the percent decomposition of HO_2NO_2. The black line represents the target temperature (~ 60 °C) for optimal separation of $CH_3O_2NO_2$ and HO_2NO_2. Rates used to calculate the fraction decomposed are shown in Table 2.

AMTD
7, 9453–9479, 2014

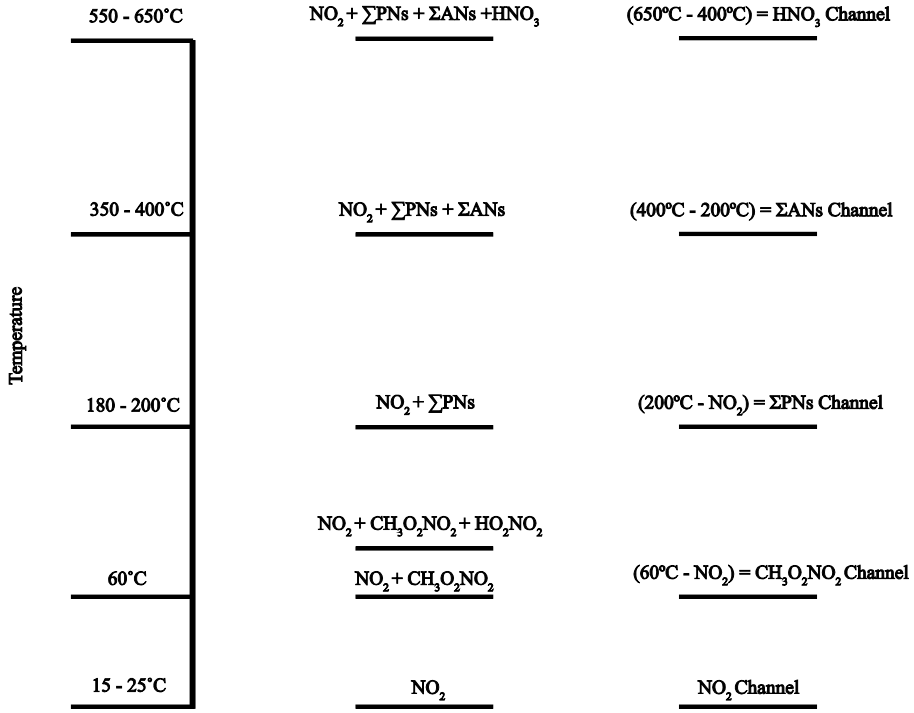

Figure 4. Schematic of the species measured in the TD-LIF channels and the temperature set points (temperatures the species dissociate) for those channels. $\Sigma PNs \equiv PAN + PPN + CH_3O_2NO_2 + HO_2NO_2 + \ldots$ and $\Sigma ANs \equiv$ alkyl and multifunctional nitrates. The channels subtracted to calculate the measured species (e.g., $CH_3O_2NO_2$) is shown before the equals sign in the third column.

AMTD
7, 9453–9479, 2014

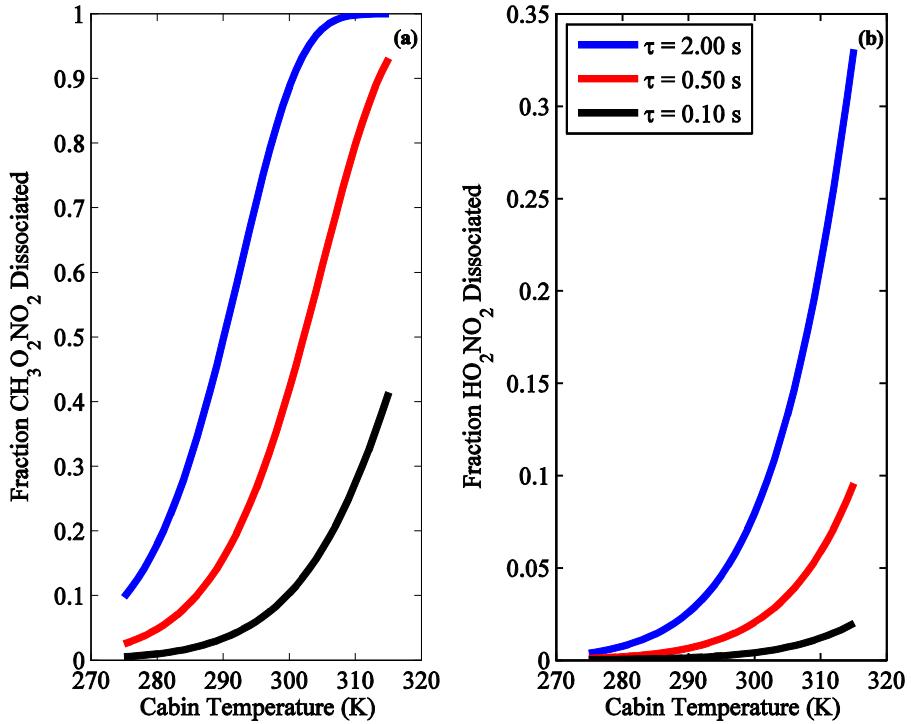

Figure 5. Calculated fraction of **(a)** $CH_3O_2NO_2$ and **(b)** HO_2NO_2 dissociated at various residence times and cabin temperatures. The calculations are for ambient pressures of 230 hPa and ambient temperatures of ~ 225 K.

AMTD
7, 9453–9479, 2014

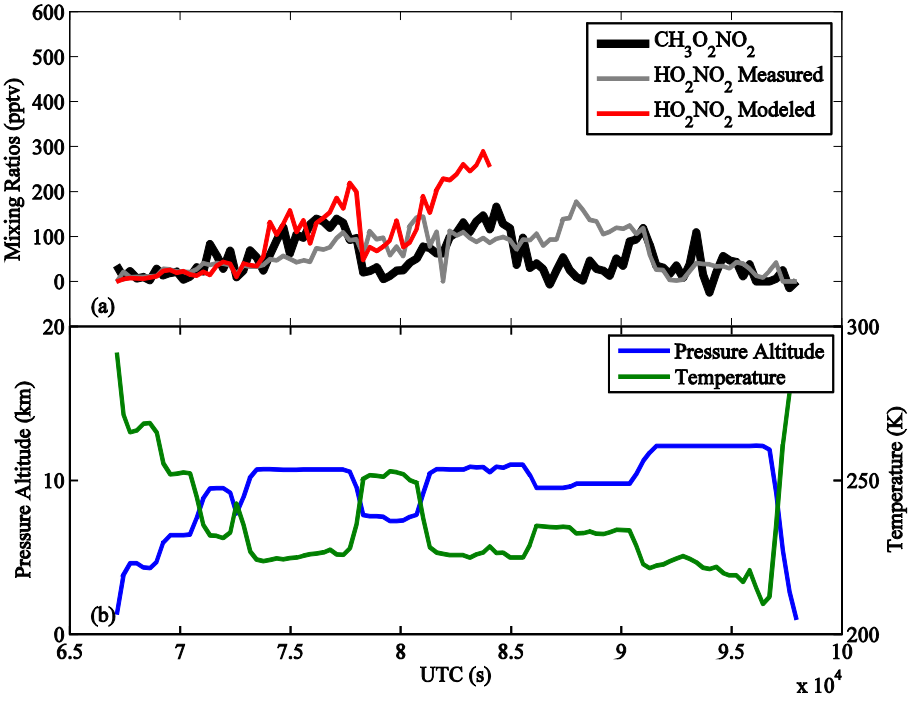

Figure 6. Five minute averaged **(a)** $CH_3O_2NO_2$ (black), HO_2NO_2 (grey) measured by chemical ionization-mass spectrometry, and HO_2NO_2 (red) calculated by photostationary steady state and divided by 2, and **(b)** pressure altitude (blue) and temperature (green) data from flight on 30 May 2012.

AMTD
7, 9453–9479, 2014

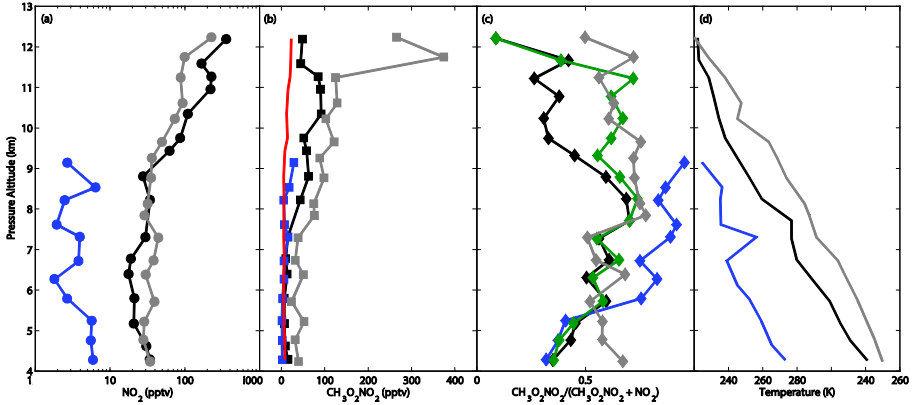

Figure 7. The median profile of **(a)** NO_2, **(b)** $CH_3O_2NO_2$, **(c)** $CH_3O_2NO_2/(NO_2 + CH_3O_2NO_2)$, and **(d)** temperature for ARCTAS-A (blue), DC-3 (black), and SEAC4RS (dark grey). The red line in **(b)** is the median limit of detection for $S/N = 2$, 60 s for DC-3. The green line in **(c)** is the median $CH_3O_2NO_2/(NO_2 + CH_3O_2NO_2)$ in background air where NO_x/NO_y is less than 0.2 during DC-3.

AMTD
7, 9453–9479, 2014

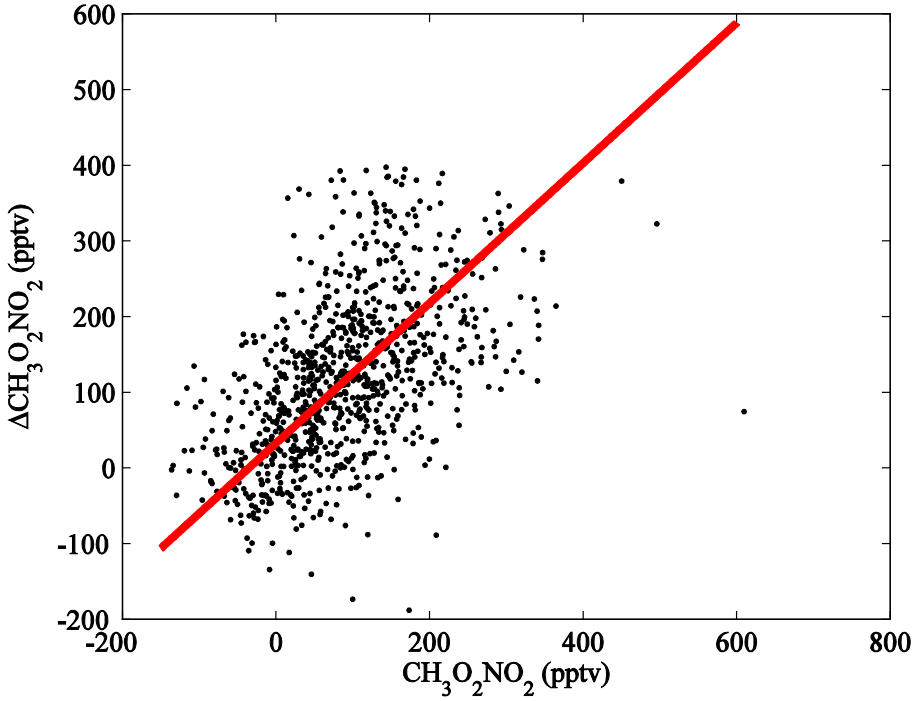

Figure 8. $CH_3O_2NO_2$ inferred ($\Delta CH_3O_2NO_2$) as the difference of the total peroxy nitrates minus PAN, PPN, and HO_2NO_2 compared to $CH_3O_2NO_2$ observed by TD-LIF at temperatures between 220 and 230 K. The red line is a weighted fit to the data: slope of 0.93 (±0.07) and intercept of −33.0 (±5.9) pptv.

AMTD
7, 9453–9479, 2014